RESEARCH ARTICLE SUMMARY

PLANT SCIENCE

Cell-by-cell dissection of phloem development links a maturation gradient to cell specialization

Pawel Roszak†, Jung-ok Heo†, Bernhard Blob†, Koichi Toyokura†, Yuki Sugiyama‡, Maria Angels de Luis Balaguer‡, Winnie W. Y. Lau‡, Fiona Hamey‡, Jacopo Cirrone‡, Ewelina Madej, Alida M. Bouatta, Xin Wang, Marjorie Guichard, Robertas Ursache, Hugo Tavares, Kevin Verstaen, Jos Wendrich, Charles W. Melnyk, Yoshihisa Oda, Dennis Shasha, Sebastian E. Ahnert, Yvan Saeys, Bert De Rybel, Renze Heidstra, Ben Scheres, Guido Grossmann, Ari Pekka Mähönen, Philipp Denninger, Berthold Göttgens, Rosangela Sozzani*, Kenneth D. Birnbaum*, Yrjö Helariutta*

INTRODUCTION: The plant root grows indeterminately. Continual birth and maturation of cells in a gradient along the root longitudinal axis requires tissue-wide coordination of cell division with cell differentiation. Within the root, a single cell file of developing protophloem is surrounded by other tissues, with each cell type differentiating at its characteristic pace. Despite communication of protophloem cells with the surrounding environment, the developmental program of phloem, within the plant's vasculature, is accelerated compared with certain surrounding cell types. Here, we take advantage of the fast pace of protophloem differentiation and the cellular changes that it undergoes to dissect its developmental trajectory using high-resolution imaging and single-cell omics.

RATIONALE: Single-cell RNA-sequencing (scRNA-seq) analysis as applied to the study of organogenesis typically creates maps of transcriptome activity in various tissue types. Although these approaches characterize gene expression within cells of an organ, the ability to reconstruct the step-by-step changes in cells during maturation is often limited. High-resolution profiling will sample each cellular state along a developmental trajectory and associate each state with developmental changes that lead to cellular specialization. To understand the developmental progression of root phloem cells at a single-cell resolution as related to cellular specializations, we used cell sorting to profile *Arabidopsis thaliana* root tissue and map protophloem-specific transcripts, scRNA-seq to identify molecular transition as cells mature, and live-cell imaging to map molecular states to morphological and cellular events during differentiation.

RESULTS: Long-term live imaging enabled us to determine the duration of the developmental stages and the time one cell spends in each position of the trajectory during protophloem sieve element maturation. We then mapped single-cell transcriptomes corresponding to the 19 cell stages of protophloem development from birth to enucleation. Combining single-cell transcriptomics with cell behavior data from live-imaging experiments, we established seven developmental phases of protophloem development, including early lineage bifurcations, transition from proliferation to differentiation, and, finally, cell enucleation.

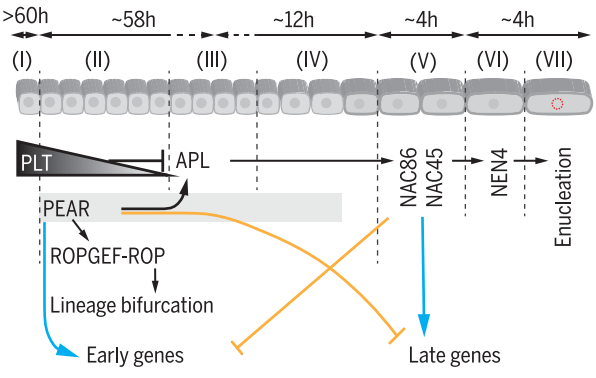

Developmental trajectory of protophloem sieve element. Interactions between transcription factors guiding protophloem sieve element development and the length of the identified developmental phases (I to VII). Arrows indicate transcriptional activation. T bars indicate transcriptional inhibition. Colored arrows depict positive and inhibitory interactions identified for early and late factors, respectively, underlying a "seesaw" model. Gray bar indicates PEAR expression domain. Wedge indicates the PLETHORA protein gradient.

The ability to connect cellular development such as lineage bifurcation and enucleation to molecular states using scRNA-seq allowed us to uncover genetic mechanisms that coordinate cellular maturation. First, our analysis revealed the importance of RHO OF PLANTS (ROP) GTPase signaling during early phloem development when the protophloem cell lineage bifurcates to generate metaphloem sieve element and procambium. We found that the expression of the phloem-enriched components of ROP GTPase signaling is triggered by lineage-specific PHLOEM EARLY DNA-BINDING-WITH-ONE-FINGER (PEAR) transcription factors. PEARs also promote phloem differentiation by transcriptional activation of the gene encoding ALTERED PHLOEM DEVELOPMENT (APL), which regulates protophloem sieve element enucleation. In the absence of PEARs, transcription of *APL*, *NAC DOMAIN CONTAINING PROTEIN 45/86* (*NAC45/86*), and *NAC45/86-DEPENDENT EXONUCLEASE-DOMAIN PROTEIN 4* (*NEN4*) is not activated in the protophloem cell lineage and cell enucleation fails.

The genetic cascade, with *PEAR*s handing off late maturation to *APL*, represents a largely autonomous phloem-specific circuit regulating maturation. However, we could also connect the timing of the genetic cascade to broadly expressed master regulators of meristem maturation. Protophloem sieve element differentiation program is temporally coordinated with the rest of the meristem by the broadly acting PLETHORA factors emanating from the stem cell niche. We showed that, although distributed across different tissues, PLETHORA factors directly repress expression of *APL*, counteracting PEARs close to the stem cell niche. The precise timing of developmental mechanisms was critical for proper phloem development; "fail-safe" mechanisms ensured orderly developmental transitions. For example, activation of late genes accompanied repression of early genes of the phloem differentiation program. Ectopic expression of selected late phloem genes in early dividing cells inhibited cell division and promoted cell expansion, two features that characterize late phloem.

CONCLUSION: Using cell sorting, live-microscopy lineage tracing, and transcriptomics, we built a high-resolution blueprint of the genetic program that guides protophloem development. We document even short developmental phases such as cell enucleation, which takes place every 2 hours. Deep, high-resolution single-cell sequencing of the underlying gene-regulatory network revealed a "seesaw" mechanism of reciprocal genetic repression that triggered rapid developmental transitions. Further analysis of this network revealed an interaction of broad versus tissue-specific transcription factors that orchestrates timing of sieve element differentiation. ■

The list of author affiliations is available in the full article online.
***Corresponding author. Email: ross_sozzani@ncsu.edu (R.S.); ken.birnbaum@nyu.edu (K.D.B.); yrjo.helariutta@helsinki.fi (Y.H.)**
†These authors contributed equally to this work.
‡These authors contributed equally to this work.
Cite this article as P. Roszak *et al.*, *Science* 374, eaba5531 (2021). DOI: 10.1126/science.aba5531

READ THE FULL ARTICLE AT
https://doi.org/10.1126/science.aba5531

RESEARCH ARTICLE

PLANT SCIENCE

Cell-by-cell dissection of phloem development links a maturation gradient to cell specialization

Pawel Roszak[1]†, Jung-ok Heo[1,2]†, Bernhard Blob[1]†, Koichi Toyokura[1,3,4,5]†, Yuki Sugiyama[1,6]‡, Maria Angels de Luis Balaguer[7]‡, Winnie W. Y. Lau[8]‡, Fiona Hamey[8]‡, Jacopo Cirrone[9]‡, Ewelina Madej[10], Alida M. Bouatta[11], Xin Wang[2], Marjorie Guichard[12,13], Robertas Ursache[1], Hugo Tavares[1,14], Kevin Verstaen[15,16], Jos Wendrich[17,18], Charles W. Melnyk[19], Yoshihisa Oda[6,20], Dennis Shasha[9], Sebastian E. Ahnert[1,21,22], Yvan Saeys[15,16], Bert De Rybel[17,18], Renze Heidstra[23], Ben Scheres[23,24], Guido Grossmann[12,13], Ari Pekka Mähönen[2], Philipp Denninger[11], Berthold Göttgens[8], Rosangela Sozzani[7]*, Kenneth D. Birnbaum[25]*, Yrjö Helariutta[1,2]*

In the plant meristem, tissue-wide maturation gradients are coordinated with specialized cell networks to establish various developmental phases required for indeterminate growth. Here, we used single-cell transcriptomics to reconstruct the protophloem developmental trajectory from the birth of cell progenitors to terminal differentiation in the *Arabidopsis thaliana* root. PHLOEM EARLY DNA-BINDING-WITH-ONE-FINGER (PEAR) transcription factors mediate lineage bifurcation by activating guanosine triphosphatase signaling and prime a transcriptional differentiation program. This program is initially repressed by a meristem-wide gradient of PLETHORA transcription factors. Only the dissipation of PLETHORA gradient permits activation of the differentiation program that involves mutual inhibition of early versus late meristem regulators. Thus, for phloem development, broad maturation gradients interface with cell-type-specific transcriptional regulators to stage cellular differentiation.

Roots consist of several concentric layers of functionally distinct cell files, which initially bifurcate and establish distinct identities around the quiescent center and its surrounding stem cells. Cells within each file mature through the distinct zones of cell proliferation and differentiation (*1*). For example, in *Arabidopsis thaliana*, the development of the protophloem sieve elements involves a transient period of cell proliferation during which, in addition to amplification of cells within the file, two lineage-bifurcating events take place (Fig. 1A) (*2*). Soon after the cell proliferation ceases, cells of the protophloem sieve element lineage initiate a differentiation process that culminates in enucleation, an irreversible process that gives rise to the mature conductive cells (*3*). Because of specific modulation of the graded distribution of the key phytohormonal cue auxin, the differentiation of protophloem sieve elements occurs faster than that of the other cell files (*4*). Therefore, protophloem sieve element development offers a tractable scheme to understand how the two processes of cell specialization and maturation interact.

Phloem developmental trajectory at single-cell resolution

To understand the process of protophloem sieve element development at a high resolution, we used a combination of approaches based on time-lapse confocal imaging (*5*) and single-cell transcriptomics (*6*). Using the phloem-specific marker *pPEAR1::H2B-YFP pCALS7::H2B-YFP*, we precisely mapped cellular behavior of the 19 cells that constitute the protophloem sieve element developmental trajectory until enucleation, which takes place every 2 hours in the final cell position. The passage of the cell from its "birth" at the stem cell until its enucleation took a minimum of 79 hours (fig. S1 and movies S1 and S2). To dissect the genetic control underlying this temporal progression, we opted for deep profiling of the 19 cells that represent the developmental trajectory of protophloem sieve element using cell sorting and well-based single-cell sequencing over higher-throughput but shallower droplet-based profiling (*6*–*12*). We used fluorescent reporter lines with expression that represents various spatiotemporal domains within the developmental trajectory of the protophloem sieve element (fig. S2, A and B). The single-cell profiles allowed us to cluster cells together with known protophloem sieve element markers to identify 758 cells that densely sampled the 19 cell positions and captured the span of protophloem sieve element maturation (Fig. 1B and fig. S2, C to G).

We sought to use the high-resolution profile of the protophloem sieve element lineage to determine how cell passage through stable signaling gradients in the meristem controls the stages of cellular specialization. In particular, whereas a number of regulators of either phloem cell identity or meristem zonation have been described (*13*, *14*), little is known about how these two regulatory processes interact to control organogenesis. Using Monocle 2 (*15*, *16*), we projected the 758 protophloem sieve element lineage cells into a pseudotemporal order and investigated transcriptional transitions along the developmental trajectory (Fig. 1, B to D). Rather than gradual changes, we observed four transcriptomic domains separated by three narrow transition zones (Fig. 1, D and E, and table S1). On the basis of the alignment with the temporal expression patterns of selected genes, we were able to determine that these domains correspond approximately to cells at positions 1 to 7 [a], 8 to 11 [b], 12 to 15 [c], and 16 to 19 [d], respectively (Fig. 1, D and E, and fig. S3). To further understand which aspects of protophloem sieve element maturation these various positions represent, we extended time-lapse confocal imaging with the more temporally specific marker lines *pNAC86::H2B-YFP* and *pNEN4::H2B-YFP*, which are active at later developmental stages (3). We found that the differentiation time, measured from the last cell division to enucleation, took ~20 hours with some variation up to the final stage defined by expression of *NAC45/86-DEPENDENT*

[1]The Sainsbury Laboratory, University of Cambridge, Cambridge, UK. [2]Institute of Biotechnology, HiLIFE/Organismal and Evolutionary Biology Research Programme, Faculty of Biological and Environmental Sciences, Viikki Plant Science Centre, University of Helsinki, Helsinki, Finland. [3]Department of Biological Sciences, Graduate School of Science, Osaka University, Osaka, Japan. [4]Faculty of Science and Engineering, Konan University, Kobe, Japan. [5]GRA&GREEN Inc., Incubation Facility, Nagoya University, Furo-cho, Chikusa-ku, Nagoya, Japan. [6]Department of Gene Function and Phenomics, National Institute of Genetics, Mishima, Japan. [7]Plant and Microbial Biology Department, North Carolina State University, Raleigh, NC, USA. [8]Wellcome Trust and MRC Cambridge Stem Cell Institute and Department of Haematology, University of Cambridge, Cambridge, UK. [9]Computer Science Department, Courant Institute for Mathematical Sciences, New York University, New York, NY, USA. [10]Faculty of Biochemistry, Biophysics and Biotechnology, Jagiellonian University, Kraków, Poland. [11]Plant Systems Biology, Technical University of Munich, Freising, Germany. [12]Institute of Cell and Interaction Biology, CEPLAS, Heinrich-Heine-University Düsseldorf, Düsseldorf, Germany. [13]Centre for Organismal Studies, Heidelberg University, Heidelberg, Germany. [14]Bioinformatics Training Facility, Department of Genetics, University of Cambridge, Cambridge, UK. [15]Data Mining and Modelling for Biomedicine, VIB Center for Inflammation Research, Ghent, Belgium. [16]Department of Applied Mathematics, Computer Science and Statistics, Ghent University, Ghent, Belgium. [17]Department of Plant Biotechnology and Bioinformatics, Ghent University, Ghent, Belgium. [18]VIB Center for Plant Systems Biology, Ghent, Belgium. [19]Department of Plant Biology, Swedish University of Agricultural Sciences, Uppsala, Sweden. [20]Department of Genetics, the Graduate University for Advanced Studies, SOKENDAI, Mishima, Japan. [21]Department of Chemical Engineering and Biotechnology, University of Cambridge, Cambridge, UK. [22]The Alan Turing Institute, British Library, London, UK. [23]Department of Plant Sciences, Wageningen University and Research, Wageningen, Netherlands. [24]Rijk Zwaan R&D, 4793 Fijnaart, Netherlands. [25]Center for Genomics and Systems Biology, New York University, New York, NY, USA.

***Corresponding author. Email: ross_sozzani@ncsu.edu (R.S.); ken.birnbaum@nyu.edu (K.D.B.); yrjo.helariutta@helsinki.fi (Y.H.)**

†These authors contributed equally to this work. ‡These authors contributed equally to this work.

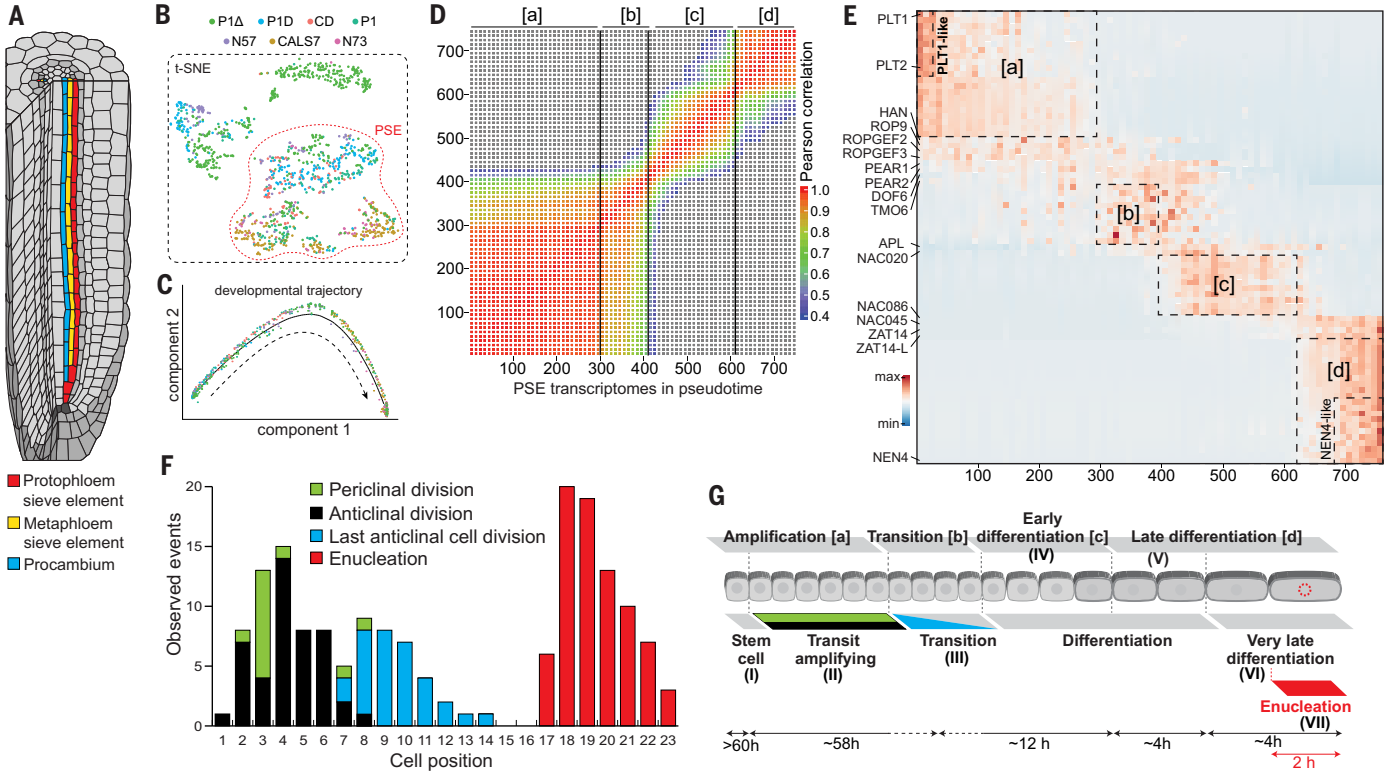

Fig. 1. Phloem development at single-cell resolution. (**A**) Schematic of the *Arabidopsis* root tip depicting the positions of the protophloem sieve element, metaphloem sieve element, and procambium cell lineages originating from a single phloem stem cell. (**B**) t-distributed stochastic neighbor embedding (t-SNE) plot of 1242 transcriptomes of cells sorted with P1Δ, P1D, CD, P1, N57, CALS7, and N73 reporter lines specific to the different domains of the developing phloem. Indicated protophloem sieve element cells were used for the pseudotime trajectory analysis (fig. S2, supplementary materials). (**C**) Protophloem sieve element transcriptomes ordered along developmental trajectory using Monocle 2. (**D**) Heatmap of Pearson correlation along the pseudotime trajectory. Vertical lines indicate the three strongest correlation drops and separate four groups of transcriptomes with higher similarity [a], [b], [c], and [d]. (**E**) Gene expression heatmap of protophloem sieve element regulators and the 10 most specific genes from the four groups defined in (D) and the nested *PLT1* ("PLT1-like") or *NEN4* ("NEN4-like") expression domains in pseudotime-ordered protophloem sieve element transcriptomes. (**F**) Histogram of cell behavior based on long-term live imaging. (**G**) Seven domains and the time cells spent in each position of the developing protophloem sieve element as determined by the transcriptomics (above) and live imaging (below): (I) "stem cell," position 1 [a], t > 60 hours; (II) "transit amplifying," positions 2 to 9 [a], t = 58 hours, SD ± 8.1 hours; (III) "transitioning, positions 8 to 11 [b]; (IV) "early differentiating," positions 10 to 15 [c], t = 12 hours; (V) "late differentiating," positions 16 and 17 [d], t = 4 hours; (VI) "very late differentiating – NEN4-like," positions 18 and 19 [d], t = 4 hours; and (VII) "enucleating," position 19 [d], t = 2 hours (movies S1 and S2).

EXONUCLEASE-DOMAIN PROTEIN 4 (*NEN4*) (active in positions 18 and 19) (Fig. 1E; fig. S1, D, H, and I; and movies S1 to S12). In summary, on the basis of the high congruence of the single-cell transcriptome and live imaging data, we were able to assign seven distinct developmental phases along the protophloem sieve element trajectory: (I) "stem cell," position 1; (II) "transit amplifying," positions 2 to 9; (III) "transitioning," positions 8 to 11; (IV) "early differentiating," positions 10 to 15; (V) "late differentiating," positions 16 and 17; (VI) "very late differentiating," positions 18 and 19; and (VII) "enucleating," position 19 (Fig. 1, F and G; fig. S1; and table S2).

PEARs promote lineage bifurcation through GTPase signaling

Proximal to the stem cell (I) developmental phase, the first distinctive feature of the protophloem sieve element lineage is the bifurcation of the procambial and metaphloem cell files from the progenitor protophloem sieve element lineage through a pair of subsequent periclinal (asymmetric) cell divisions in the domain of transit amplifying cells (II). Using the single-cell lineage and imaging analysis, we sought to precisely map these divisions (Fig. 2A). We observed that the first periclinal division followed exclusively a rare event of phloem stem cell division (movie S13 and fig. S4A). The second, more frequent, periclinal division was observed predominantly at position 3 (Fig. 1F). We have recently shown that the PHLOEM EARLY DNA-BINDING-WITH-ONE-FINGER (PEAR) transcription factors (TFs) (transcribed in domains I to IV) mediate early asymmetric divisions in the phloem lineage and laterally adjacent procambial cells in a cell-autonomous and non-cell-autonomous manner, respectively (*17*).To identify potential downstream effector genes for this PEAR function, we focused on the genes enriched in the expression domain of *pPEAR1Δ::erVenus* marker line (see the materials and methods), capturing the bifurcation events and the resulting protophloem, metaphloem, and procambium cell lineages (Fig. 2B and fig. S4B).

Among the sieve element–enriched genes that were highly expressed in single-cell profiles preceding and during the bifurcation (domain II), we identified and validated the protophloem sieve element abundant expression of Rho-related guanosine triphosphatase (GTPase), Rho of plants 9 (ROP9) (*18*), as well as several genes encoding PRONE-type ROP guanine nucleotide exchange factors (ROPGEF) (Fig. 2, B to D, and fig. S4, B, C, and F) (*19*). ROP GTPase signaling controls the polarity of the multiple cell types during cell differentiation (*20*–*22*) and specific cell division events (*23*–*25*). Subsequently, we determined that ROPGEF3 and ROPGEF5 expression in the protophloem

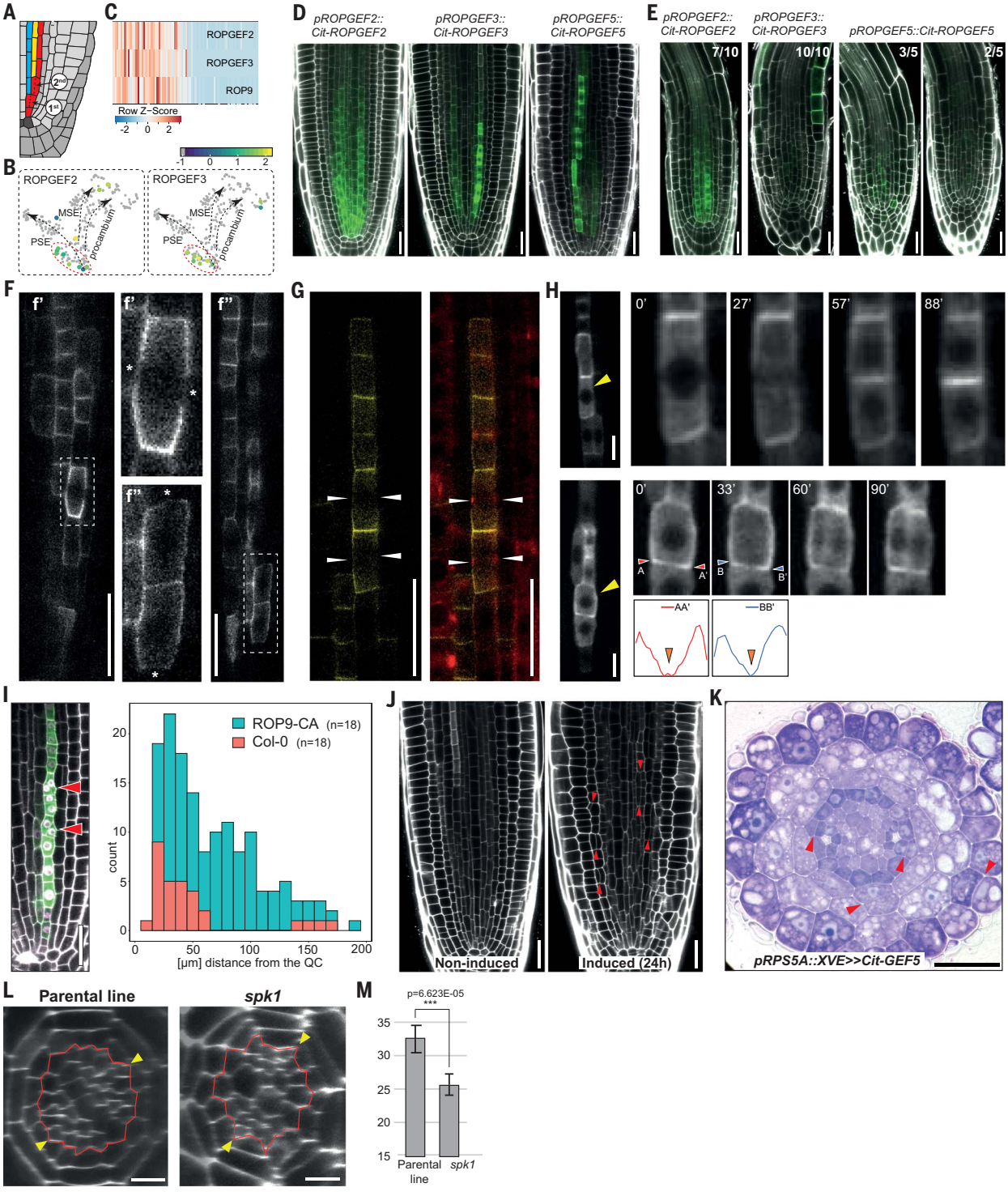

Fig. 2. PEARs control asymmetric divisions by promoting ROP signaling in the phloem pole. (**A**) Schematic indicating position of the two periclinal divisions in the phloem cell lineage. (**B**) Expression of ROPGEF2 and ROPGEF3 at the time of phloem lineage bifurcation. (**C**) Peak expression of ROPGEF2, ROPGEF3, and ROP9 in the early phloem cells as detected in the pseudotime-ordered single-cell protophloem sieve element transcriptome data. (**D**) Expression pattern of phloem-enriched ROPGEFs. ROPGEF3, and ROPGEF5 share similar expression domains, which are enriched in protophloem sieve element and adjacent vascular cell files; ROPGEF2 is expressed in protophloem sieve element but also in other outer procambial cells and pericycle (fig. S4D). Scale bars, 25 µm. (**E**) Expression of ROPGEF2, ROPGEF3, and ROPGEF5 in the *pear* sextuple mutant background. Scale bars, 25 µm. (**F**) Protein localization of *pROPGEF5::Cit-ROPGEF5* during anticlinal (f') and periclinal (f'') cell division. Gaps in ROPGEF5 signal are indicated with an asterisk. Scale bars, 25 µm. (**G**) Depletion of Cit-ROPGEF5 membrane signal at the cortical division zone (CDZ) during cell division. CDZ is marked by accumulating cortical microtubules (mCherry-TUA5) forming a pre-prophase band (white arrowheads). Scale bars, 25 µm. (**H**) Time course analysis of the dynamic pattern of active ROP signaling in the dividing phloem cells. Depletion of *pPEAR1::mScarlet-I-MIDD1ΔN* signal at the CDZ in the anticlinally (upper row) and periclinally (lower row) dividing cells (yellow arrowheads). Quantification of

fluorescence signal intensity in the periclinally dividing cells. Scale bars, 10 μm. (**I**) Quantification of asymmetric cell divisions (red arrowheads) in the protophloem sieve element cell lineage after expression of constitutively active ROP9 (Q64L) (*pPEAR1::XVE>>ROP9^{CA}*). Scale bars, 25 μm. (**J**) Ectopic asymmetric cell divisions (red arrowheads) 24 hours after induction of ectopic Cit-GEF5 expression (*pRPS5A::XVE>>Cit-GEF5*). Scale bars, 25 μm. (**K**) Toluidine blue staining of resin sections of a Cit-GEF5–overexpressing line (*pRPS5A::XVE>>Cit-GEF5*) 24 hours after induction. Red arrowheads indicate ectopic periclinal cell divisions in epidermis, endodermis, and pericycle. Scale bars, 25 μm. (**L**) Identification of *spk1* allele in the mutant screen of *pRPS5A::PEAR1-GR* parental line. Presented are images from noninduced plants. Scale bars, 10 μm. (**M**) Quantification of vascular cell files in the *spk1* mutant and its parental line *pRPS5A::PEAR1-GR*. Neither line was induced, *t* test indicates statistical difference.

sieve element lineage is dependent upon PEAR factors, based on the spatiotemporal correlation as well as the analysis of transcriptional reporters in the *pear* sextuple mutant background (Fig. 2E). In addition, functional analysis of the PEAR-binding sites previously indicated by the DNA affinity purification sequencing (DAP-seq) technique (*26*) in the promoter region of ROPGEF genes affected their expression level (fig. S4D) (17), suggesting a direct interaction.

In the dividing cells, ROPGEFs accumulated broadly at the cell membrane but were depleted from the expected position of the cortical division zone, which demarcates the future division plane (Fig. 2F) (*25*). Indeed, observed gaps in ROPGEF localization coincided with the position of microtubule array called the preprophase band, the earliest marker of the cell division plane in plants (Fig. 2G and fig. S4E) (*25*). ROPGEFs catalyze the disassociation of GDP from an inactive ROP-GDP complex that enables quick binding of free cytosolic GTP and thus activates ROP signaling. In the active state, ROP-GTP interacts with a number of different effector proteins to mediate downstream signaling (*27*). To detect the cellular position of the active ROP signaling in relation to the periclinal and anticlinal cell division planes in phloem, we used a molecular biosensor of ROP signaling that consists of the fluorescently tagged, ROP-GTP–binding domain from the MICROTUBULE DEPLETION DOMAIN1 (MIDD1ΔN) effector protein (*28*). Similar to the localization of ROPGEFs, subcellular localization of active ROP signaling was detected on the cell membrane and was absent in the cortical division zone of protophloem sieve element cells during mitosis (Fig. 2H).

To test whether ROP signaling plays a decisive role in the selection of the cell division plane, we generated an inducible line expressing the constitutively active form of ROP9 (ROP9^{CA}) (see the materials and methods) and lines ectopically expressing phloem-enriched ROPGEFs. Accumulation of ROP9^{CA}-3xYFP on the radial walls of the protophloem sieve element lineage correlated with cell expansion to the radial direction and reorientation of the cell division plane (Fig. 2I and fig. S4F). Ectopic expression of ROPGEFs resulted in ectopic periclinal cell divisions in the outer root layers and pericycle, which rarely undergo such division (Fig. 2, J and K, and fig. S4, G and H). Members of the PRONE-type ROPGEF gene family in *Arabidopsis* have previously been proposed to act redundantly in a number of processes in which they activate ROP signaling (*29*). However, loss of *SPIKE1* (*SPK1*), encoding a single-copy ROP-interacting DOCK family GEF, causes phenotypes mimicking the combinatorial *rop* mutants (*30*–*32*). Therefore, we focused on the loss-of-function alleles of *SPK1*, one of which we identified in the genetic screen for factors promoting formative (periclinal) cell divisions (see the supplementary materials). In the *spk1* loss-of-function mutant, we detected a reduction in periclinal divisions in several tissues, including the protophloem sieve element cell lineage (Fig. 2, L and M, and fig. S4, I to K). We conclude that in the transit amplifying cells (domain II, positions 2 to 9), PEAR function promotes the bifurcation involving the emergence of the protophloem sieve element cell lineage by switching the orientation of the cell divisions at least partially through the activation of ROPGEF-ROP signaling module.

PLETHORAs stage *APL* expression and phloem differentiation

Another distinctive feature of the early protophloem sieve element developmental trajectory is the transition from cell division to cell differentiation (domain II to III to IV). This transition mapped closely to the first major change in the protophloem sieve element transcriptome. In the first transcriptomic domain (domain I to II), we detected transcripts of the PLETHORA gene family (Fig. 1E), the relatively persistent proteins of which are known to spread shootward through cell-to-cell movement. This movement, together with a mitotic dilution effect, contributes to the formation of the shootward protein gradient of PLETHORAs (*14*). Prior work has shown that PLETHORA TFs broadly regulate meristem development, promoting cell division at moderate concentrations, and then permitting elongation and differentiation as levels drop (*14*, *33*, *34*). However, it is not clear how individual cell files interpret the meristem-wide PLETHORA gradient for their own specialized differentiation.

We hypothesized that the PLETHORA gradient might mediate the first transcriptional shift (from domain II to III) toward protophloem sieve element differentiation by permitting a new set of transcripts to be expressed (Fig. 3A). We tested this hypothesis by driving PLETHORA2 (PLT2) under several promoters that extended its expression in the protophloem sieve element in later maturation stages than its native domain (Fig. 3B and fig. S5A). When using the *pNAC86::XVE* inducible promoter, which is active in domains V to VII (*3*, *35*), ectopic PLT2 delayed protophloem sieve element enucleation (Fig. 3B and fig. S5A). Transcriptional profiling of phloem cells expressing the construct showed an up-regulation of genes (table S3) that mapped to the early stages of the protophloem sieve element single-cell trajectory (from domain I to II), the known PLT2 protein gradient (Fig. 3C). These results suggest that extending the PLT2 gradient is sufficient to prolong the early stages of meristem maturation within the protophloem sieve element lineage, providing a connection between the maturation of a specific cell file and a meristem-wide protein gradient. In addition, in the pseudo-time ordered single cells, we could detect complementary oscillatory patterns of the putative S-phase and G_2- to M-phase genes that were also among the up-regulated PLETHORA targets, apparently corresponding to regular progressions through the cell cycle (Fig. 3C and fig. S5B). Furthermore, *ALTERED PHLOEM DEVELOPMENT* (*APL*), *NAC45/86*, and *NEN4*, known key regulators of the protophloem sieve element enucleation pathway (*3*), were among the PLT2–down-regulated genes (fig. S5C and table S3). This is consistent with the presence of *APL* in the large set of genes down-regulated by PLETHORA overexpression (*33*). We validated the down-regulation of *APL* and *NEN4* by ectopic *PLT2* expression with in situ hybridization (Fig. 3D and fig. S5D). We also monitored a shootward shift of *APL* expression domain in the roots after conditional ectopic induction of *PLT2* expression. The induction of PLT2 in the phloem cells beyond its native domain confirmed that activation of APL-dependent genetic program requires dissipation of the PLETHORA gradient (Fig. 3E). To determine the role of PLETHORAs in controlling the transition between transit amplification and differentiation in phloem, we used an inducible, tissue-specific CRISPR/Cas9 approach to mutate *PLT2* specifically in the protophloem sieve element cell file (*36*). We observed an acceleration of the protophloem sieve element differentiation, as well as the expression of *pAPL::erTurq* reporter, toward the quiescent center without affecting the broader meristem size or root growth, showing

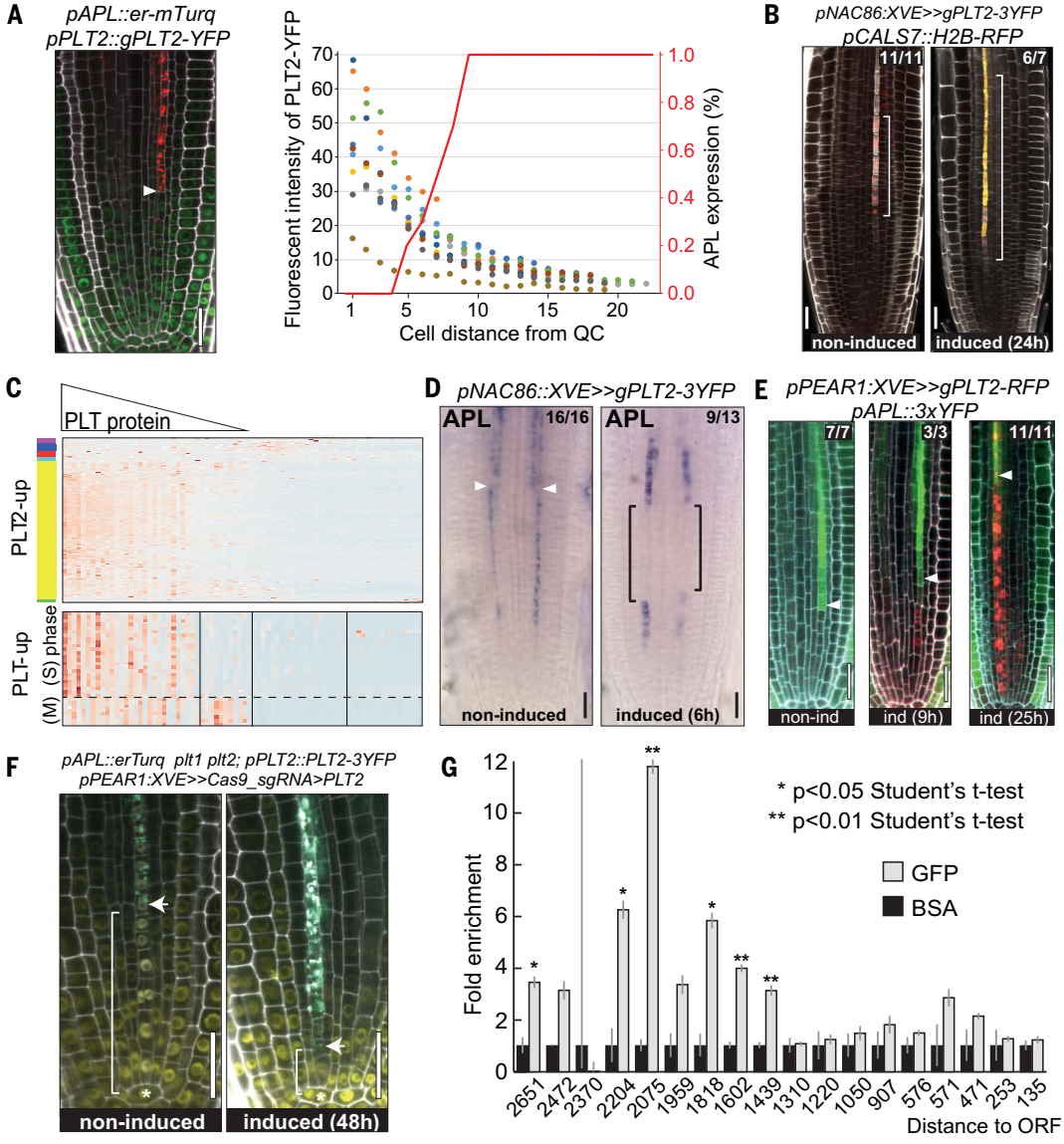

Fig. 3. PLT2 inhibits phloem differentiation by directly repressing APL expression. (**A**) Quantification of the fluorescent intensity of PLT2-YFP in protophloem sieve element cells of nine roots indicated with dots of different colors. Percentage of roots expressing *APL* in a given protophloem sieve element cell is indicated as a red line (n = 9). Onset of *APL* expression coincides with diminishing level of PLT2 protein. Arrowhead indicates the onset of *APL* expression in the protophloem sieve element. (**B**) Ectopic expression of *PLT2* under the *pNAC86::XVE* promoter delays protophloem sieve element enucleation. Square brackets indicate extended expression domain of *pCALS7::H2B-RFP*, a reporter used for monitoring enucleation. (**C**) Native expression profile of PLT2 targets in protophloem sieve element cells ordered in pseudotime. Genes up-regulated after 6 hours of induction of the line shown in (B) are plotted. Upper panel shows gradually diminishing expression of target genes, which reflects the PLT2 protein gradient. Lower panel shows PLT2 up-regulated cell cycle genes with an oscillatory expression pattern. (**D**) In situ hybridization of *APL* before and 6 hours after ectopic expression of PLT2-3xYFP. Arrowheads indicate the positions of protophloem sieve element enucleation beyond which point *APL* is expressed in the phloem pole pericycle, companion cells, and the metaphloem sieve element (fig. S5E). Brackets indicate the *pNAC086* activity domain. (**E**) Time course of transcriptional repression of *APL* in cells ectopically expressing PLT2-RFP under the inducible *pPEAR1::XVE* promoter. (**F**) Early activation of *APL* expression 48 hours after phloem-specific knockout of *PLT2*. (**G**) ChIP-qPCR of PLT2-3xYFP on the *APL* promoter revealing the PLETHORA-binding region −2204 to −1439 bp upstream of the *APL* ORF. All scale bars, 25 μm.

that loss of PLETHORA function in its native domain allows precocious expression of mid- to late-stage protophloem sieve element differentiation regulators (Fig. 3F and fig. S5, F to H).

We sought to further test whether PLT2 directly regulates the protophloem sieve element–specific differentiation program because we found AP2 (a member of the PLETHORA family) family–binding sites in the *APL* promoter region, as determined by the DAP-seq technique (*26*). Indeed, we confirmed the direct binding of PLT2 to several regions of the *APL* promoter by chromatin immunoprecipitation (ChIP) followed by quantitative PCR (qPCR) (Fig. 3G). Furthermore, along with AP2 sites, the *APL* promoter is also enriched for binding sites of HANABA TANARU (HAN), a GATA TF. In turn, *HAN* is a PLETHORA target (*33*) and, accordingly, upon ectopic PLT2 expression we detected *HAN* transcripts expressed in late protophloem sieve element development (fig. S5, C and I). Ectopic HAN expression under *pNAC86:XVE* led to a delay in enucleation (fig. S5J), similar to PLT2 overexpression in the same domain. We conclude that the PLETHORA gradient directly (and possibly in a feedforward manner with HAN) orchestrates protophloem sieve element differentiation by cell autonomously repressing transcription of the phloem regulator *APL*. Overall, our results show how the PLETHORA gradient first promotes cell proliferation in the protophloem sieve element lineage and then helps to time the later stages of cellular maturation.

PEARs promote *APL* to orchestrate phloem differentiation

Given the results above, we reasoned that an early phloem-specific TF must activate *APL* expression. To identify genes that could fill that role, we first generated a list of sieve element genes enriched in our bulk-sorted cells from that tissue compared with published data profiling other tissue types of the root meristem [(*37*); fig. S6A and table S4]. We further narrowed the list by intersecting it with sieve element–enriched genes identified in the cluster analysis of single-cell RNA-sequencing

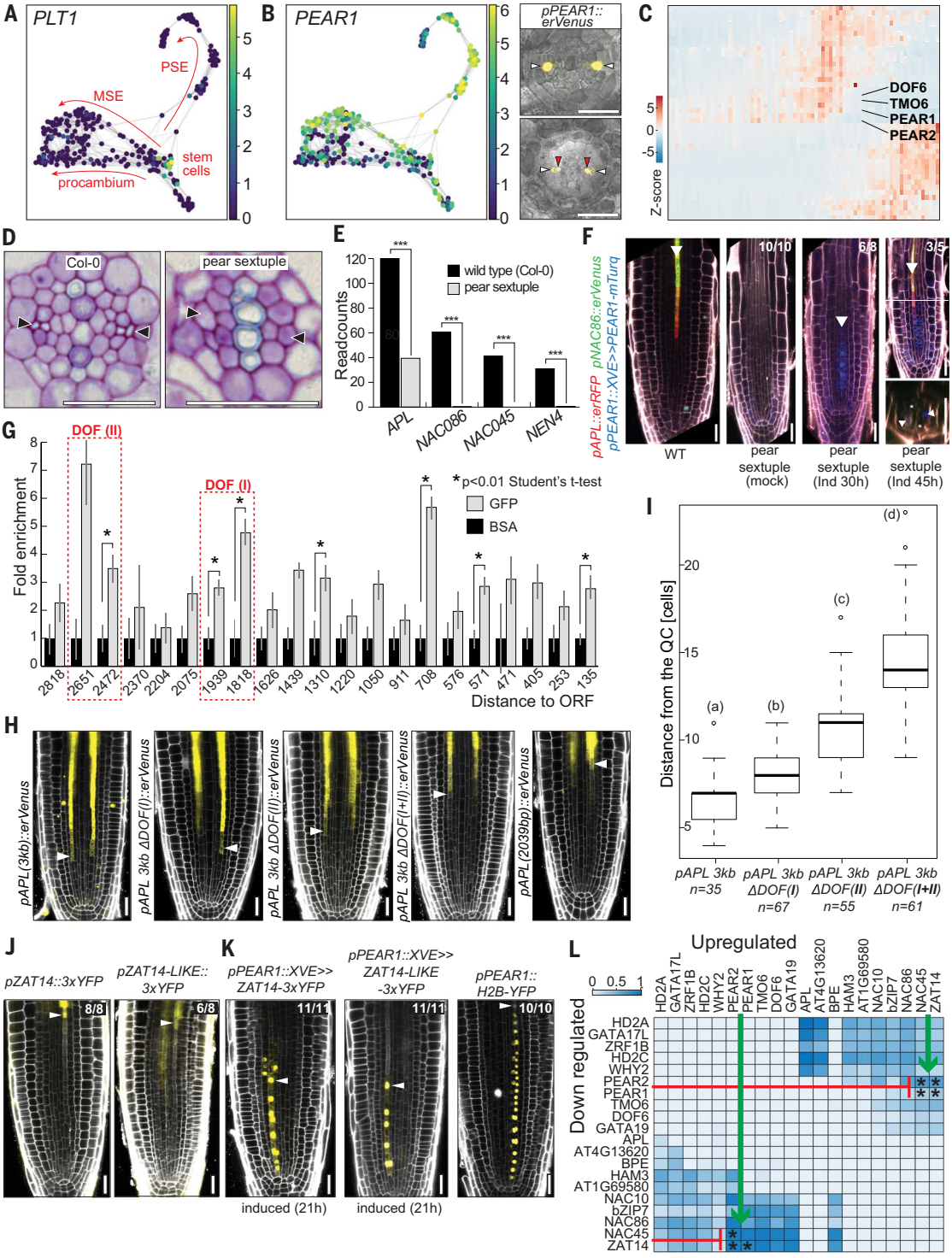

Fig. 4. PEARs orchestrate phloem differentiation. (**A**) Force-directed clustering of 272 single-cell transcriptomes obtained using the *pPEAR1Δ::erVenus* reporter. Plotted is the expression of stem cell–abundant *PLT1*. Arrows indicate cellular trajectories inferred from known gene expression patterns (fig. S6). (**B**) Strong enrichment of *PEAR1* expression in protophloem sieve element and metaphloem sieve element trajectories confirmed by the *pPEAR1::erVenus* reporter line. White arrowheads indicate the protophloem sieve element and red arrowheads the metaphloem sieve element. (**C**) Expression heatmap. PEAR genes are among the earliest phloem-specific TFs. (**D**) Lack of protophloem sieve element differentiation in the mature part of the *pear* sextuple mutant root. Arrowheads indicate the protophloem sieve element position. (**E**) Lack of *APL* pathway activation in the roots of *pear* sextuple mutant based on RNA-seq analysis. (**F**) Inducible expression of *PEAR1-mTurq* is sufficient to activate transcription of *APL* and *NAC86* reporters in the *pear* sextuple mutant background. (**G**) ChIP-qPCR of PEAR1-YFP shows a direct interaction of PEAR1 with *APL* promoter at multiple positions. Two prominent PEAR1-binding sites are indicated with red dashed rectangles. (**H**) Expression patterns of modified *pAPL* reporter lines. Length of the "3kb" promoter equals 2962 bp. DOF(I) and DOF(II) correspond to the two enhancer elements indicated in (G). Details of this modification are provided in fig. S7C. (**I**) Quantification of the onset of *pAPL* expression after

modification of DOF-binding motives. Statistically significant differences between groups were tested using Tukey's post hoc test, $P < 0.05$. Different letters indicate a significant difference at $P < 0.05$. (**J**) Expression of ZAT14 and ZAT14L during late differentiation of protophloem sieve element. Arrowheads indicate the last cell before enucleation. (**K**) Ectopic expression of *ZAT14* and *ZAT14L* under *pPEAR1::XVE* results in cell elongation and inhibition of cell division. Arrowheads indicate the last cell before enucleation. The *pPEAR1::H2B-YFP* line shows the regular number of protophloem sieve element cells. (**L**) Heatmap showing significantly overlapping and oppositely regulated target sets of the 20 most important TFs from the gene-regulatory network model. Color intensity shows the fraction of overlapping target sets. The colormap represents significantly overlapping sets (Fisher's exact test, if $P < 0.05$, value = 1) multiplied by the fraction of overlap. Asterisk indicates experimental validation of up- and down-regulated sets from TF overexpression in vivo (tables S15 and S16). All scale bars, 25 μm.

(scRNAseq) profiles of the *pPEAR1Δ::erVenus* reporter line (table S5; Fig. 4, A and B; and fig. S6, B to H). From this analysis, we identified 542 sieve element–enriched genes (table S6) and corroborated their specificity in the published whole-root scRNAseq atlas (table S7) (*12*). We modeled gene regulation using a machine-learning approach on the pseudotime-ordered 758 single-cell profiles and 4924 highly variable genes. Among the 208 TFs in this dataset, most of the known protophloem sieve element TFs (such as *APL*, *NAC045*, and *NAC086*) were among the top 20 regulators (table S8). We validated the model by comparing predicted targets with genes induced by in vivo ectopic expression of the same TFs, confirming a significant overlap of targets in three of five cases (table S8). Among the top 20 regulators, we also identified four related genes that encode early sieve element–abundant PEAR TFs (*PEAR1*, *PEAR2*, *DNA BINDING WITH ONE FINGER6*, and *TARGET OF MONOPTEROS6*) (Fig. 4C). We recently showed that simultaneous loss of six PEAR genes results in defects in protophloem sieve element differentiation (*17*). We subsequently profiled the transcriptomes of wild-type and *pear* sextuple mutant (Fig. 4D) root meristems and identified 203 down-regulated genes overlapping with our protophloem sieve element–specific gene list (table S9). The expression of *APL*, as well as its downstream targets *NAC045*, *NAC086*, and *NEN4*, was lost in the protophloem tissue of the *pear* sextuple mutant (Fig. 4, E and F, and fig. S7A). Subsequently, expression of *APL* and *NAC086* reporter lines was restored in the pear sextuple mutant upon induction of *PEAR1*, corroborating that transcriptional activation of *APL* in the protophloem sieve element is dependent on the activity of PEAR factors (Fig. 3F).

To test whether PEAR1 can directly regulate the expression of *APL* in its endogenous expression domain (cells 1 to 14), we performed ChIP followed by qPCR using *pPEAR1::PEAR1-GFP* protein fusion and identified multiple PEAR1-binding sites within the *APL* promoter (*pAPL*) (Fig. 4G). Truncation analysis of *pAPL* indicated the presence of an enhancer element responsible for the expression of *APL* in the cells transitioning from cell division to cell differentiation within the 2039- to 2962-bp region upstream of the *APL* open reading frame (ORF) (Fig. 4H). Our ChIP analysis detected a single strong PEAR1-GFP peak in the promoter sequence beyond 2039 bp from the ORF and another strong peak at the upstream end of the 2-kb region, both of which were also detected in the publicly available DAP-seq data (Fig. 4G and fig. S7C) (*26*). Furthermore, within the detected regions (−2672 to −2512 and −1946 to −1844), we identified multiple clusters of DOF-binding motifs (AAAG) (*26*) that constitute an enhancer element required for the transcriptional activation of *APL* in the phloem transition zone (domain III) (Fig. 4, H and I, and fig. S7C). Although the expression of *APL* in the protophloem sieve element is dependent on PEARs (Fig. 4F), *APL* expression domain extends beyond *PEAR* domain (cells 15 to 19; Fig. 1E and fig. S3A). It is possible that either the PEAR proteins and/or *APL* mRNA persist during this period ~10 hours before enucleation. Alternatively, there may be intermediate factors acting downstream of PEARs to promote *APL* expression during late stages of phloem development. Collectively, the data support a role for PEARs in controlling the onset of APL expression to regulate a transition in phloem differentiation. The transition is controlled by the PLETHORAs, which dissipates its own gradient by promoting cell division. When PLETHORA levels decline sufficiently, PEARs can then effectively up-regulate *APL*. The opposing regulation of *APL* by positively regulating PEARS and inhibitory PLETHORAs illustrates how antagonistic mechanisms, one forming a morphogen-like gradient across the meristem, orchestrate developmental timing within a cell file.

Sequential mutual inhibition directs developmental transitioning

The final major transcriptional transition in the phloem lineage occurs between domains IV and V. To explore this transition, we ectopically expressed NEN4 and PLT2 at various developmental stages. When expressed in early ectopic domains, NEN4 expression caused cell death, whereas PLT2 expression forced cells back into the cell cycle. However, later expression of these two TFs had little or no visible effect on cells, showing that the developmental program of domain V appears to be resilient to these perturbations (Fig. 3B and figs. S5A and S9). This indicates that the high number of protophloem sieve element–specific genes during the final 8 hours of differentiation remodel the cellular behavior in an irreversible manner. We next sought to explore how widely the PEARs control transcriptional programs related to this final stage of sieve element development. We combined a gene-regulatory analysis in the *pear* mutant with systematic overexpression and modeling approaches (fig. S7, A and B, and fig. S8). Our analysis revealed that, in addition to the known phloem regulators *APL*, *NAC045*, *NAC086*, and *NAC028*, 10 of 13 newly validated phloem-enriched TFs were dependent on PEARs (fig. S7, A and B, and Fig. 4F). Overexpression of two of these, *ZAT14* (AT5G03510), which was also the third most important TF in the machine-learning model, and its close homolog *ZAT14L* (AT5G04390), led to the arrest of cell cycle and premature cell elongation (Fig. 4, J and K). Transcriptional profiling provided further evidence for a putative dual role in timing cell division and cell expansion (that occurred largely after enucleation in this cell lineage) (tables S10 to S14). In addition, the gene-regulatory network model predicted a pattern of sequential mutual inhibition in the target sets of high-scoring transcriptional regulators (table S15); for example, genes repressed by ZAT14 significantly overlapped with genes activated by the earlier expressed PEARs and vice versa (Fig. 4L). Overexpression analysis confirmed a significant overrepresentation in the overlap between genes up-regulated by PEARs and down-regulated by ZAT14 (table S16) (*17*).

By combining single-cell transcriptomics with live imaging, we have mapped the cellular events from the birth of the phloem cell to its terminal differentiation into phloem sieve element cells spanning a time frame of 79 hours. In the early part of the developmental trajectory, where cells are proliferating, the PEAR factors promote the asymmetric periclinal divisions that result in lineage bifurcation. We pinpoint the ROPGEF-ROP–regulatory module as an effector of early PEAR function in promoting the periclinal cell divisions central to vascular development. In addition, the PEARs activate the final 20-hour terminal differentiation program, which highlights them as central integrators that connect early and late phloem development. Our high-resolution phloem developmental trajectory reveals three abrupt transitions in the gene expression program. The late, PEAR-regulated protophloem sieve element program is directly and antagonistically controlled by the broad PLETHORA

gradient, which connects this morphogen-like gradient to cellular maturation. We propose that mutual inhibition of target genes by sequentially expressed TFs represents a "seesaw" mechanism (fig. S10) that allows rapid transitions and prevents gene expression programs with conflicting effects on cellular physiology (e.g., division versus enucleation). Similar models have been implicated in so-called attractor states in cell fate decisions in animals (*38*). In the future, it will be interesting to determine how conserved these principles of sieve element differentiation are in an evolutionary context, as well as how extensively they apply to other differentiation trajectories in plants.

Methods summary

The single-cell transcriptomic data described herein were generated from the protophloem and metaphloem sieve element, and procambial cells, which were sorted using tissue-specific fluorescent reporter lines. Root tips of 5-day-old *Arabidopsis* plants were used as a tissue material for protoplasting. RNA sequencing of the sorted cells was performed following a well-based Smart-seq protocol. Obtained transcriptomes, corresponding to the cells from the protophloem cell lineage, were ordered in pseudotime using the Monocle 2 package, which generated a single linear protophloem developmental trajectory. Expression profiles and pseudotime coordinates of the known phloem-expressed genes were further confirmed with in situ and reporter line analyses.

The gene-regulatory network was modeled using a random forest machine-learning approach. Selected interactions, representing mutual inhibition (the seesaw model), were confirmed by the transcriptome analysis of lines overexpressing a candidate gene or profiling of the loss-of-function lines.

To understand cell behavior at different developmental phases, confocal long-term live imaging was performed with the protophloem sieve element–specific and nuclear localized reporter line. Up to 5-day-long movies were recorded, and cell behavior, including the number and position of cell divisions, enucleation, and times of these events were recorded.

All details of the methods, including those summarized above, are provided in the supplementary materials.

REFERENCES AND NOTES

1. L. Dolan *et al*., Cellular organisation of the *Arabidopsis thaliana* root. *Development* **119**, 71–84 (1993). doi: 10.1242/dev.119.1.71; pmid: 8275865
2. A. P. Mähönen *et al*., A novel two-component hybrid molecule regulates vascular morphogenesis of the *Arabidopsis* root. *Genes Dev.* **14**, 2938–2943 (2000). doi: 10.1101/gad.189200; pmid: 11114883
3. K. M. Furuta *et al*., Plant development. *Arabidopsis* NAC45/86 direct sieve element morphogenesis culminating in enucleation. *Science* **345**, 933–937 (2014). doi: 10.1126/science.1253736; pmid: 25081480
4. P. Marhava *et al*., A molecular rheostat adjusts auxin flux to promote root protophloem differentiation. *Nature* **558**, 297–300 (2018). doi: 10.1038/s41586-018-0186-z; pmid: 29875411
5. R. Rahni, K. D. Birnbaum, Week-long imaging of cell divisions in the *Arabidopsis* root meristem. *Plant Methods* **15**, 30 (2019). doi: 10.1186/s13007-019-0417-9; pmid: 30988691
6. I. Efroni *et al*., Root Regeneration Triggers an Embryo-like Sequence Guided by Hormonal Interactions. *Cell* **165**, 1721–1733 (2016). doi: 10.1016/j.cell.2016.04.046; pmid: 27212234
7. T. Denyer *et al*., Spatiotemporal developmental trajectories in the *Arabidopsis* root revealed using high-throughput single-cell RNA sequencing. *Dev. Cell* **48**, 840–852.e5 (2019). doi: 10.1016/j.devcel.2019.02.022; pmid: 30913408
8. C. N. Shulse *et al*., High-throughput single-cell transcriptome profiling of plant cell types. *Cell Rep.* **27**, 2241–2247.e4 (2019). doi: 10.1016/j.celrep.2019.04.054; pmid: 31091459
9. K. Jean-Baptiste *et al*., Dynamics of gene expression in single root cells of *Arabidopsis thaliana*. *Plant Cell* **31**, 993–1011 (2019). doi: 10.1105/tpc.18.00785; pmid: 30923229
10. T.-Q. Zhang, Z.-G. Xu, G.-D. Shang, J.-W. Wang, A single-cell RNA sequencing profiles the developmental landscape of *Arabidopsis* root. *Mol. Plant* **12**, 648–660 (2019). doi: 10.1016/j.molp.2019.04.004; pmid: 31004836
11. K. H. Ryu, L. Huang, H. M. Kang, J. Schiefelbein, Single-cell RNA sequencing resolves molecular relationships among individual plant cells. *Plant Physiol.* **179**, 1444–1456 (2019). doi: 10.1104/pp.18.01482; pmid: 30718350
12. J. R. Wendrich *et al*., Vascular transcription factors guide plant epidermal responses to limiting phosphate conditions. *Science* **370**, eaay4970 (2020). doi: 10.1126/science.aay4970; pmid: 32943451
13. M. Bonke, S. Thitamadee, A. P. Mähönen, M.-T. Hauser, Y. Helariutta, APL regulates vascular tissue identity in *Arabidopsis*. *Nature* **426**, 181–186 (2003). doi: 10.1038/nature02100; pmid: 14614507
14. A. P. Mähönen *et al*., PLETHORA gradient formation mechanism separates auxin responses. *Nature* **515**, 125–129 (2014). doi: 10.1038/nature13663; pmid: 25156253
15. C. Trapnell *et al*., The dynamics and regulators of cell fate decisions are revealed by pseudotemporal ordering of single cells. *Nat. Biotechnol.* **32**, 381–386 (2014). doi: 10.1038/nbt.2859; pmid: 24658644
16. X. Qiu *et al*., Reversed graph embedding resolves complex single-cell trajectories. *Nat. Methods* **14**, 979–982 (2017). doi: 10.1038/nmeth.4402; pmid: 28825705
17. S. Miyashima *et al*., Mobile PEAR transcription factors integrate positional cues to prime cambial growth. *Nature* **565**, 490–494 (2019). doi: 10.1038/s41586-018-0839-y; pmid: 30626969
18. P. Winge, T. Brembu, R. Kristensen, A. M. Bones, Genetic structure and evolution of RAC-GTPases in *Arabidopsis thaliana*. *Genetics* **156**, 1959–1971 (2000). doi: 10.1093/genetics/156.4.1959; pmid: 11102387
19. A. Berken, C. Thomas, A. Wittinghofer, A new family of RhoGEFs activates the Rop molecular switch in plants. *Nature* **436**, 1176–1180 (2005). doi: 10.1038/nature03883; pmid: 15980860
20. Y. Fu, Y. Gu, Z. Zheng, G. Wasteneys, Z. Yang, *Arabidopsis* interdigitating cell growth requires two antagonistic pathways with opposing action on cell morphogenesis. *Cell* **120**, 687–700 (2005). doi: 10.1016/j.cell.2004.12.026; pmid: 15766531
21. A. J. Molendijk *et al*., *Arabidopsis thaliana* Rop GTPases are localized to tips of root hairs and control polar growth. *EMBO J.* **20**, 2779–2788 (2001). doi: 10.1093/emboj/20.11.2779; pmid: 11387211
22. Y. Oda, H. Fukuda, Initiation of cell wall pattern by a Rho- and microtubule-driven symmetry breaking. *Science* **337**, 1333–1336 (2012). doi: 10.1126/science.1222597; pmid: 22984069
23. J. A. Humphries *et al*., ROP GTPases act with the receptor-like protein PAN1 to polarize asymmetric cell division in maize. *Plant Cell* **23**, 2273–2284 (2011). doi: 10.1105/tpc.111.085597; pmid: 21653193
24. P. Yi, G. Goshima, Rho of Plants GTPases and cytoskeletal elements control nuclear positioning and asymmetric cell division during Physcomitrella patens branching. *Curr. Biol.* **30**, 2860–2868.e3 (2020). doi: 10.1016/j.cub.2020.05.022; pmid: 32470363
25. D. Stöckle *et al*., Putative RopGAPs impact division plane selection and interact with kinesin-12 POK1. *Nat. Plants* **2**, 16120 (2016). doi: 10.1038/nplants.2016.120; pmid: 27501519
26. R. C. O'Malley *et al*.. *Cell* **165**, 1280–1292 (2016). doi: 10.1016/j.cell.2016.04.038; pmid: 27203113
27. G. Feiguelman, Y. Fu, S. Yalovsky, ROP GTPases structure-function and signaling pathways. *Plant Physiol.* **176**, 57–79 (2018). doi: 10.1104/pp.17.01415; pmid: 29150557
28. Y. Sugiyama, M. Wakazaki, K. Toyooka, H. Fukuda, Y. Oda, A novel plasma membrane-anchored protein regulates xylem cell-wall deposition through microtubule-dependent lateral inhibition of rho GTPase domains. *Curr. Biol.* **27**, 2522–2528.e4 (2017). doi: 10.1016/j.cub.2017.06.059; pmid: 28803875
29. P. Denninger *et al*., G. Distinct RopGEFs successively drive polarization and outgrowth of root hairs. *Curr. Biol.* **29**, 1854–1865.e5 (2019). doi: 10.1016/j.cub.2019.04.059; pmid: 31104938
30. J. L. Qiu, R. Jilk, M. D. Marks, D. B. Szymanski, The *Arabidopsis* SPIKE1 gene is required for normal cell shape control and tissue development. *Plant Cell* **14**, 101–118 (2002). doi: 10.1105/tpc.010346; pmid: 11826302
31. D. Basu, J. Le, T. Zakharova, E. L. Mallery, D. B. Szymanski, A SPIKE1 signaling complex controls actin-dependent cell morphogenesis through the heteromeric WAVE and ARP2/3 complexes. *Proc. Natl. Acad. Sci. U.S.A.* **105**, 4044–4049 (2008). doi: 10.1073/pnas.0710294105; pmid: 18308939
32. H. Ren *et al*., SPIKE1 activates ROP GTPase to modulate petal growth and shape. *Plant Physiol.* **172**, 358–371 (2016). doi: 10.1104/pp.16.00788; pmid: 27440754
33. C. Galinha *et al*., PLETHORA proteins as dose-dependent master regulators of *Arabidopsis* root development. *Nature* **449**, 1053–1057 (2007). doi: 10.1038/nature06206; pmid: 17960244
34. L. Santuari *et al*., The PLETHORA gene regulatory network guides growth and cell differentiation in *Arabidopsis* roots. *Plant Cell* **28**, 2937–2951 (2016). doi: 10.1105/tpc.16.00656; pmid: 27920338
35. R. Siligato *et al*., MultiSite Gateway-compatible cell type-specific gene-inducible system for plants. *Plant Physiol.* **170**, 627–641 (2016). doi: 10.1104/pp.15.01246; pmid: 26644504
36. X. Wang *et al*., An inducible genome editing system for plants. *Nat. Plants* **6**, 766–772 (2020). doi: 10.1038/s41477-020-0695-2; pmid: 32601420
37. S. Li, M. Yamada, X. Han, U. Ohler, P. N. Benfey, High-resolution expression map of the *Arabidopsis* root reveals alternative splicing and lincRNA regulation. *Dev. Cell* **39**, 508–522 (2016). doi: 10.1016/j.devcel.2016.10.012; pmid: 27840108
38. J. Shu, H. Deng, Lineage specifiers: New players in the induction of pluripotency. *Genomics Proteomics Bioinformatics* **11**, 259–263 (2013). doi: 10.1016/j.gpb.2013.09.005; pmid: 24095709

ACKNOWLEDGMENTS

We thank Y. Kondo, P. Benfey, and O. Leyser for providing seeds of *pNAC57::2GFP*, *pSHR::erGFP*, and *pPIN4::PIN4-GFP* reporters, respectively; the staff of the Flow Cytometry Core Facility at CIMR for technical support with cell sorting; S. Fujita (National Institute of Genetics, Japan) for providing pDONRP2rP3_MIDD1ΔNcds_stop vector; and R. Wightman and G. Evans for technical support with microscopy experiments. **Funding:** This work was supported by Finnish CoE in Molecular Biology of Primary Producers (Academy of Finland CoE program 2014-2019) decision 271832 (Y.H.); the Gatsby Foundation GAT3395/PR3 (Y.H.); University of Helsinki award 799992091 (Y.H.); ERC Advanced Investigator grant SYMDEV 323052 (Y.H.); NSF-BBSRC MCSB grant 1517058 (R.S. and Y.H.); NSF CAREER MCB grant 1453130 (R.S.); NIH grant GM078279 (K.D.B.); NFS IOS grant 1934388 (K.D.B. and D.S.); NIH grant R35GM136362 (K.D.B.); MRC Clinical Research Infrastructure award MR/M008975/1 (B.G.); core funding from the Wellcome and MRC to the Cambridge Stem Cell Institute (B.G.); Academy of Finland grants 266431 and 307335 (A.P.M. and X.W.); NWO Horizon grant 050-71-054 (R.H.); ERC Starting Grant TORPEDO 714055 (B.D.R.); Research Foundation – Flanders (FWO) Odysseus II GOD0515N (B.D.R.); A Gatsby Foundation CDF grant (S.E.A.); A BOF postdoctoral fellowship from Ghent University (J.R.W.); Wallenberg Academy Fellowship KAW 2016.0274 (C.W.M.); Wellcome Strategic Award 105031/D/14/Z (F.H.); A JSPS Research Fellowship for Young Scientists (K.T.); JSPS KAKENHI grant JP16J00131 (K.T.); a JSPS Overseas Research Fellowship (Y.S.); MEXT KAKENHI grants 16H06280 and 19H05677 (Y.O.); and the Finnish Academy of Science (J.H.). This research was funded, in whole or in part, by the Wellcome Trust (203151/Z/16/Z) and the UKRI Medical Research Council (MC_PC_17230). **Authors contributions:** Conceptualization: P.R., J.H., B.B., K.T., Y.S., M.A.d.L.B., J.C., P.D., G.G., R.H., B.S., C.W.M., B.G., A.P.M., R.S.,

K.D.B., Y.H.; Methodology: J.C., X.W., Y.O., A.M.B., M.G.; Investigation: P.R., J.H., B.B., K.T., Y.S., W.W.Y.L., R.U., E.M.; Data analysis: P.R., J.H., B.B., K.T., Y.S., M.A.d.L.B., F.H., J.C., H.T., K.V., J.W., Y.S., B.D.R., S.E.A., D.S., K.D.B.; Writing: P.R., J.H., B.B., K.D.B., Y.H. **Competing interests:** The authors declare no competing interests. **Data and materials availability:** All data are available in the supplementary materials. Raw RNA-sequencing data for pooled (bulk-sorted) protophloem sieve element cells, single protophloem sieve element cells, and overexpression and mutant profiling have been deposited at the Gene Expression Omnibus of the National Center for Biotechnology Information (submissions GSE142259, GSE140778, and GSE140977, respectively). For the purpose of open access, the author has applied for a CC BY public copyright license to any author-accepted manuscript version arising from this submission.

SUPPLEMENTARY MATERIALS

science.org/doi/10.1126/science.aba5531
Materials and Methods
Figs. S1 to S10
Tables S1 to S20
Movies S1 to S13
References (*39*–*53*)
MDAR Reproducibility Checklist

View/request a protocol for this paper from *Bio-protocol*.

19 December 2019; resubmitted 8 September 2021
Accepted 10 November 2021
10.1126/science.aba5531